Journal of Nuclear Materials 383 (2008) 78–85

Contents lists available at ScienceDirect

Journal of Nuclear Materials

journal homepage: www.elsevier.com/locate/jnucmat

Microstructural and textural developments during Zircaloy-4 fuel tube fabrication

K.V. Mani Krishna [a], S.K. Sahoo [b], I. Samajdar [b,*], S. Neogy [a], R. Tewari [a], D. Srivastava [a], G.K. Dey [a], Gaur Hari Das [c], N. Saibaba [c], S. Banarjee [a]

[a] Materials Science Division, Bhabha Atomic Research Center, Trombay, Mumbai 400085, India
[b] Department of Metallurgical Engineering and Materials Science, Indian Institute of Bombay, Mumbai 400076, India
[c] Nuclear Fuel Complex, Hyderabad, India

A B S T R A C T

Developments in crystallographic texture and in microstructure were characterized during the fabrication steps of Zircaloy-4 fuel tube. Textural developments were generalized in terms of $\langle 10\bar{1}0\rangle$ and (0001) fibers. These two fibers were observed to get enhanced by the processes of deformation and annealing respectively. Microstructural evolution, on the other hand, ranged from bimodal grain size and shape distribution of the hot extruded stage, to visible heterogeneous deformation associated with pilgering and to fully or partially recrystallized structures after annealing. Textural evolution, associated with individual processing steps during both deformation as well as annealing, had a stronger contribution from relatively larger grains.

1. Introduction

Majority of in-core structural components of thermal nuclear reactors are made up of zirconium based alloys [1]. Reliable performance of these components under aggressive reactor environment imposes stringent requirements on properties [2–14] and dimensional tolerances [2]. Zircaloy-4 tubes, used for sheathing the fuel elements, depend largely for their in-service performance on microstructural features like grain morphology, grain size distribution, crystallographic texture, nature and distribution of precipitates, etc. Such microstructural aspects greatly influence irradiation creep, hydride precipitation and reorientation, etc. [3–14]. Hence it is essential to have an efficient processing flow sheet that results in components with suitable microstructure, leading to optimized short and long term properties with required dimensional tolerances.

Thermomechanical processing (TMP) steps [15–33] used for the fabrication of zirconium components are aimed at obtaining required dimensional tolerances and optimized microstructure. The structural evolution at each of these TMP steps is important. Firstly, the texture and microstructure at the end of one stage decides ease or difficulty of the next stage of processing [1]. Secondly, the final microstructure, and associated properties, is often a cumulative outcome of series of changes occurring at each stage of processing [1,24]. Hence, characterizations [16–26] of microstructural developments associated with TMP stages of zirconium tubes assumes importance in optimization of processing parameters.

In general the fabrication route of Zircaloy-4 clad tubes consists of 4 pilgering steps with intermediate annealings. In the present study, a modified route consisting of 3 pilgering and intermediate annealings steps was adopted for the fabrication of clad tubes (Fig. 1). The modification is aimed at increasing the production rate and yield. A systematic characterization of the microstructural and textural evolution in each of the stages of the new route is presented in the subsequent sections. The possible micro mechanisms leading to the observed microstructural evolutions are discussed.

2. Experimental

The chemical composition of Zircaloy-4, used in this study, is given in Table 1. Samples were drawn, for detailed characterization, from each of the stages shown in Fig. 1. In the present study, XRD, Electron Back Scattered Diffraction (EBSD) and Transmission Electron Microscopy (TEM) techniques were used for bulk texture, microtexture, and microstructural characterization, respectively.

Samples were prepared using standard metallographic techniques of mechanical and electropolishing for bulk and micro textural measurements. Bulk texture measurements were conducted on a Panalytical MRD system and the orientation distribution functions (ODFs) were estimated using commercial software Labosft. In the case of 'as cast' sample bulk texture measurements were not attempted due to excessive grain size of the order of few millimeters. EBSD measurements were conducted using a Fei Quanta-200 HV Scanning Electron Microscope (SEM) and a TSL-OIM system. At least a total area of $800 \times 200\ \mu m^2$ was scanned in each

* Corresponding author. Tel./fax: +91 22 578 3480.
E-mail address: indra@met.iitb.ac.in (I. Samajdar).

0022-3115/$ - see front matter © 2008 Published by Elsevier B.V.
doi:10.1016/j.jnucmat.2008.08.050

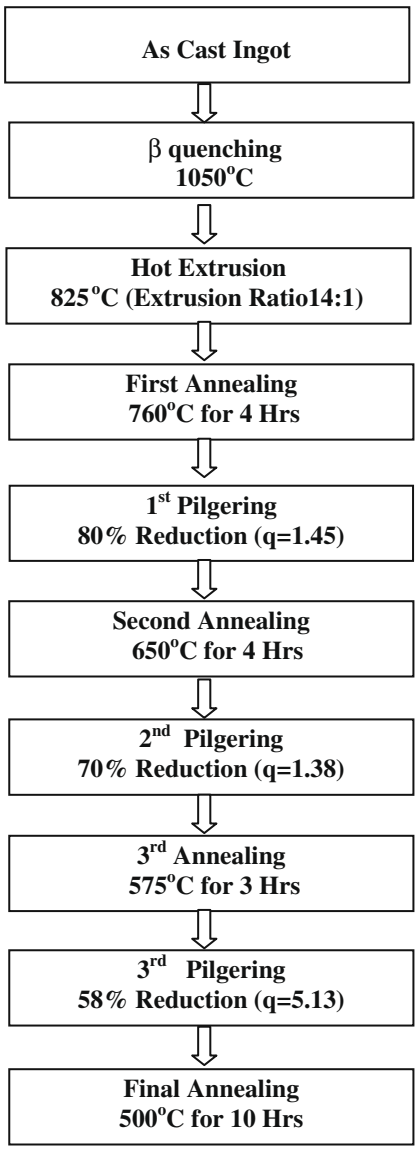

Fig. 1. The TMP flow sheet of Zircaloy-4 fuel tube used in the present study. '*q*' represents the ratio of thickness strain to radial strain for the corresponding pilgering step.

Table 1
Chemical composition of Zircaloy-4 clad tubes used in the present study

Element	Sn	Fe	Cr	Al	Hf	C	Zr
Amount by weight	1.32%	0.2%	0.1%	39.0 ppm	<50 ppm	<55 ppm	Balance

sample. A step size of 0.5 μm was used for scans. For TEM studies, a JEOL 2000FX TEM was used.

3. Results

The results on bulk crystallographic texture and on microstructure/microtexture are presented separately.

3.1. Bulk crystallographic texture

Three dimensional ODFs for samples taken from different TMP stages – starting from 'β-quenching' to 'final annealing' are shown in Fig. 2. It can be seen from the figure that TMP stages did undertake strong developments/modifications in crystallographic texture. Randomized 'β-quenched' texture was converted to relatively well defined 'hot extruded' texture, which was then modified through successive deformation/pilgering and annealing stages. This fact is shown more clearly in the Fig. 3 which depicts $\varphi_2 = 30°$ sections of ODFs.

It is apparent from the ODFs (see Figs. 2 and 3), that two families of fiber orientations define the textural developments/modifications associated with TMP stages. These are $\langle 10\bar{1}0\rangle$ and (0001) fibers. Fig. 4 describes the textural developments in terms of the changing volume fractions of these fibers. Deformation during hot extrusion and pilgering, strengthened $\langle 10\bar{1}0\rangle$, while annealing strengthened (0001). The only exception to this generalized pattern was during the third pilgering, where the increase in $\langle 10\bar{1}0\rangle$ fiber was insignificant. It, however, needs to be noted that the third pilgering involved lowest reduction and also the highest '*q*' value.[1]

3.2. Microstructure and microtexture

EBSD and TEM observations are classified in three segments – microstructure evolution up to hot extrusion, pilgered structures and annealed structures. These are described through figures, Figs. 5–7, and listed sequentially in the following sub-sections.

3.2.1. Microstructure evolution up to hot extrusion

Very large grains (several millimeters) of the 'as cast' structure (Fig. 5(a)) did get refined (100 μm and lower) through β-quenching (Fig. 5(b)). In addition, β-quenching provided Widmanstätten morphology. Hot extrusion, developed a clear bimodal distribution in grain size and in grain morphology. (Fig. 5(c)) It exhibited larger elongated grains in association with smaller equiaxed grains. Micro textural analysis of these grains brought out following important observations (Table 2):

- Elongated larger grains had higher grain average misorientation and were observed to contain (qualitatively) more dislocation density (Fig. 7(a)).
- Larger grains, in general, contained more intermetallics precipitates.
- Larger grains were more textured.

3.2.2. Pilgered structures

The main observation on the pilgered structures can be stated in a single point to be 'heterogeneous deformation', (Fig. 5(e)). As apparent in the EBSD scans, majority of the grains were fragmented (i.e. formation of high angle boundaries and also large dislocation density; the latter can be seen through the TEM image, Fig. 7(b)). However, few grains/orientations were non-fragmented. The latter type of grains clearly contributed to textural evolution, see Fig. 6. Microstructures corresponding to second and third pilgering, qualitatively similar to Fig. 5(e), are not included. It may be pointed out that the second and third pilgering produced similar 'heterogenous deformation', albeit with less number of indexable points and of non-fragmented grains.

3.2.3. Annealed structures

Microstructural/microtextural evolutions associated with annealing steps can be summarized as:

[1] '*q*' value represents thickness strain vs. radial strain. A high '*q*' takes the strain path closer to near plane strain.

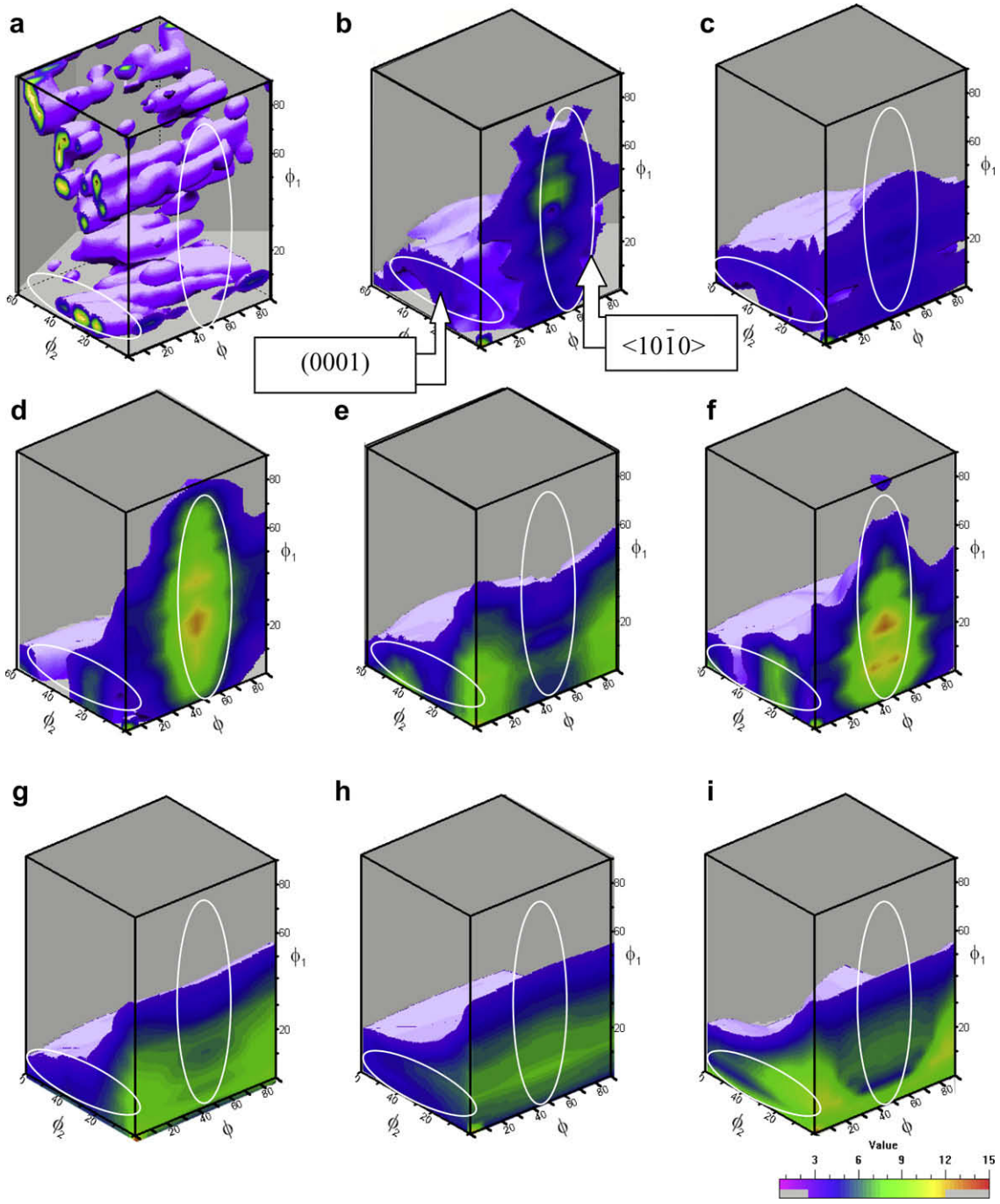

Fig. 2. Three dimensional ODF plots for (a) β-quenched , (b) hot extruded, (c) first annealed, (d) first pilgered, (e) second annealed, (f) second pilgered, (g) third annealed, (h) third pilgered and (i) final annealed. ODF iso-intensity levels of three times or more are marked. The two distinct fibers, $\langle 10\bar{1}0\rangle$ and (0001) fibers, are shown on the ODFs.

- 'First annealed' structure hints at recovery/recrystallization (minor, but consistent, drop in grain average misorientation (GAM) values were recorded) and also at grain coarsening (an increase in average grain size of 9–12 μm from hot extruded structure). Bimodal grain size distribution remained (Fig. 5(d)), though the large grains were, in general, less elongated.
- 'Second Annealing', produced a fully recrystallized (estimation based on GAM) equiaxed microstructure of 8 μm average grain size (Fig. 5(f)).
- 'Third annealing' and 'final annealing' resulted in a partially recrystallized microstructures (Fig. 5(g) and (h)), extent of recrystallization (as estimated by GAM and grain size distribution) being less in case of 'final annealing'. The partially recrystallized nature of 'final annealed' microstructure was also revealed by TEM observations (Fig. 7(c)).
- Larger grains, in general, had stronger contribution towards texture developments/evolution – see Fig. 6.

4. Discussion

Textural and microstructural evolution associated with TMP stages of zirconium is a subject of strong technological and academic importance [16–26,28–36]. Hot extrusion, often a critical

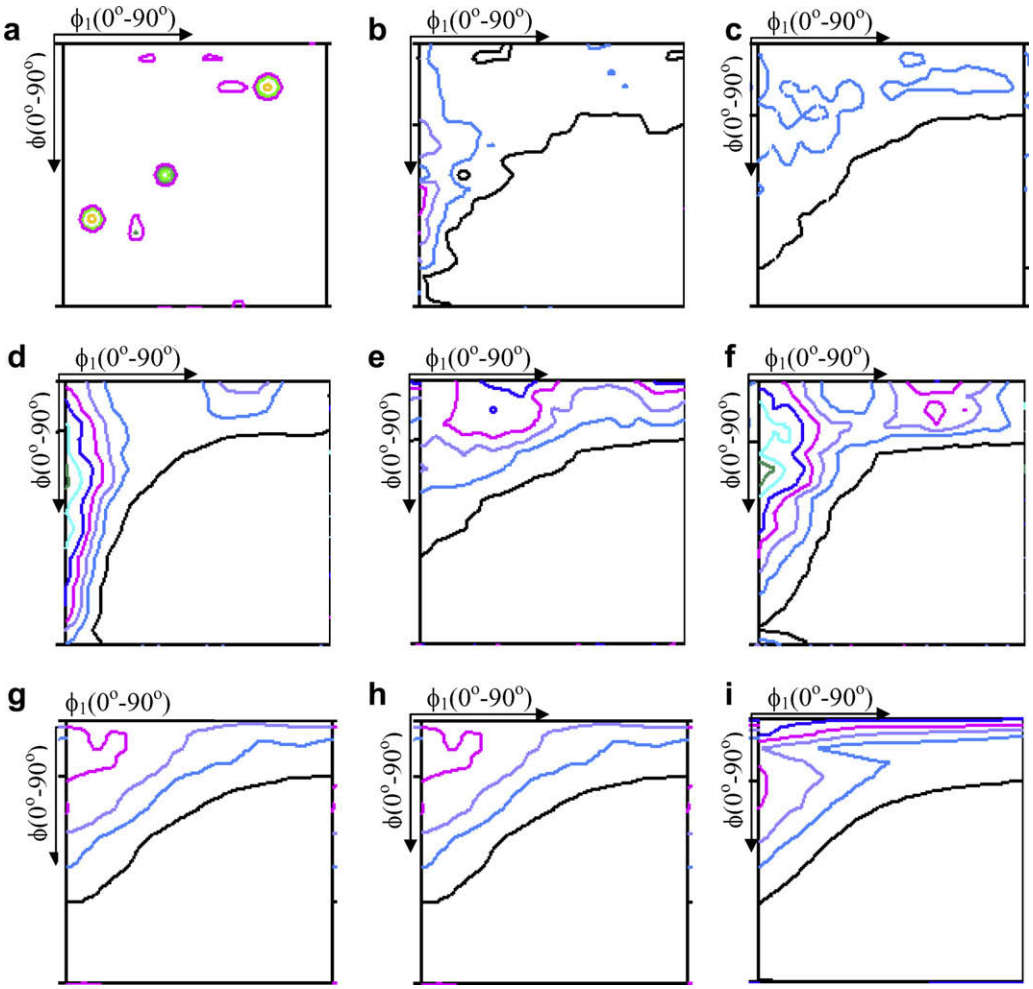

Fig. 3. $\varphi_2 = 30°$ sections of ODF for (a) β-quenched , (b) hot extruded, (c) first annealed, (d) first pilgered, (e) second annealed , (f) second pilgered, (g) third annealed, (h) third pilgered and (i) final annealed. Contor levels are marked at 5, 6, 7, 10, 11 and 12 times random.

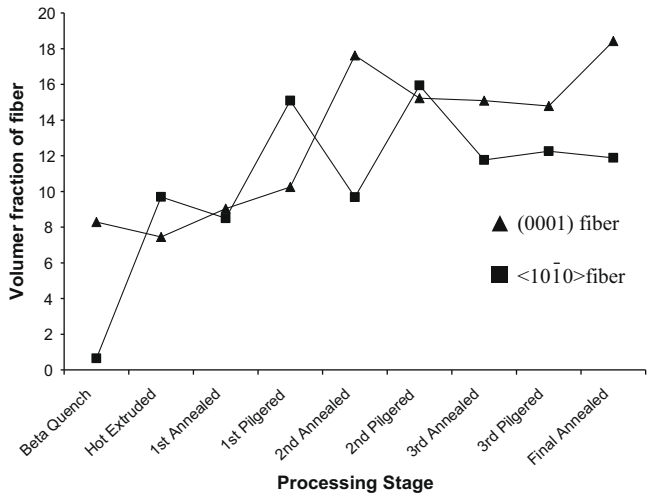

Fig. 4. Volume fractions of the important fibers, $\langle 10\bar{1}0\rangle$ and (0 0 0 1), as a function of processing steps.

step, is recognized [2,16,18,28–30] to bring about maximum textural development. Present study also showed the importance of 'hot extrusion' in bringing about well defined crystallographic texture from a randomized 'β-quenched' texture. Subsequent TMP stages have induced systematic modifications on the hot extruded texture. Quantification of textural developments, in terms of idealized $\langle 10\bar{1}0\rangle$ and (0001) fibers indicated a clear pattern: in general deformation (both hot extrusion as well as pilgering) is associated with strengthening of $\langle 10\bar{1}0\rangle$, while (0001) fiber got enhanced during annealing steps. These observations are in good agreement with reported cold deformation and annealing fibers of single phase zirconium alloys [1,26]. Though previous studies indicated deformation to be more important in textural developments, present study clearly showed annealing also had a significant contribution to textural modifications (see Figs. 2–4).

Present study, based on EBSD measurements, provided a strong correlation between observed bulk crystallographic texture and microstructure/microtexture. In general, larger grains had a prominent contribution to the textural evolution during deformation/pilgering as well as annealing, see Fig. 6. In the pilgered structures (Fig. 5(e)), larger grains were identified as non-fragmenting. These are the grains where formation of new grain boundaries were not observed. It is important to point out that a recent study [34] had produced clear evidence of 'heterogeneous deformation' in near plane strain deformed Zircaloy-2. Two classes of grains/orientations were identified – generalized as 'deforming' and 'non-deforming', the latter did not undergo refinement in grain size (or grain fragmentation), had significantly lower GAM and also lower macroscopic strain (as estimated through changes in aspect ratio). The pilgered structures of the present Zircaloy-4 appears similar, except for the fact that the non-fragmenting grains were 'elongated'. In any case, deformation of single phase zirconium,

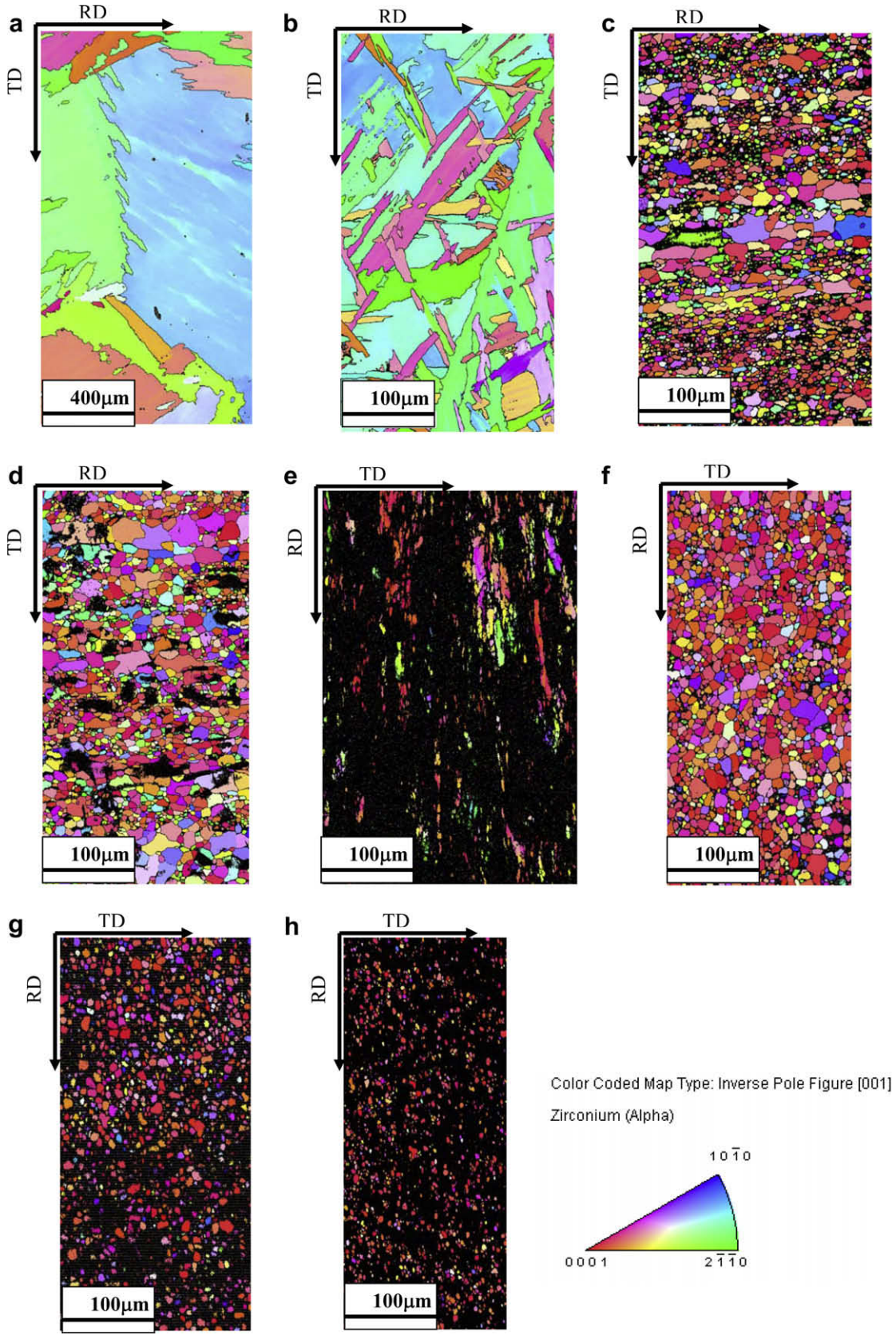

Fig. 5. EBSD images of (a) as cast (b) β-quenched, (c) hot extruded, (d) first annealed, (e) first pilgered, (f) second annealed, (g) third annealed and (h) final annealed. Images were plotted using inverse pole figure convention – grain boundaries being marked for above 15° misorientation. Measurement points with confidence index (an approximate measure of accuracy of indexing) values below 0.03 are marked as black. RD & TD correspond respectively to axial and circumferential directions of the tube.

both Zircaloy-2 under near plane strain or Zircaloy-4 under pilgering with different '*q*', shows clear evidence of 'heterogeneous deformation'. Stronger texture evolution is clearly associated with larger or non-fragmenting grains.

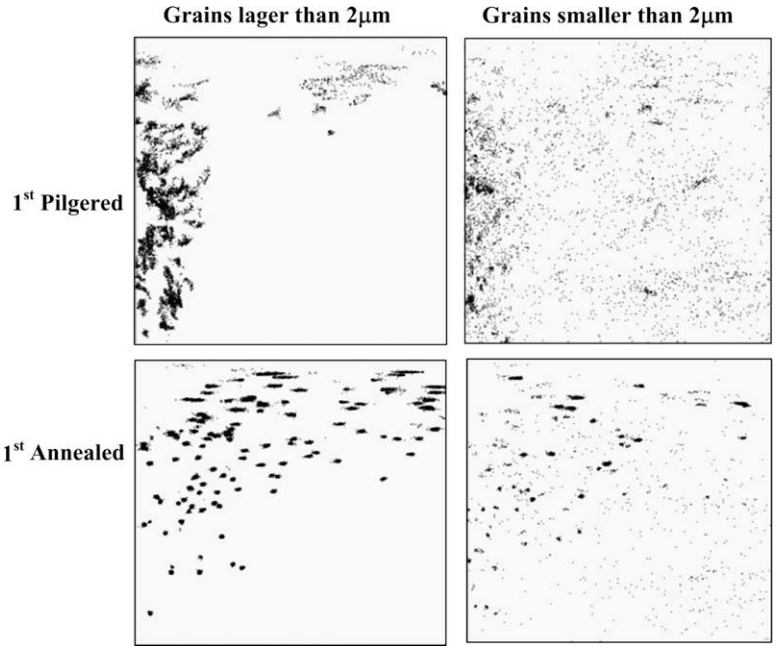

Fig. 6. $\varphi_2 = 30^\circ$ sections of Euler space for 'first pilgered' and 'first annealed' samples showing that larger grains were more textured than the smaller ones.

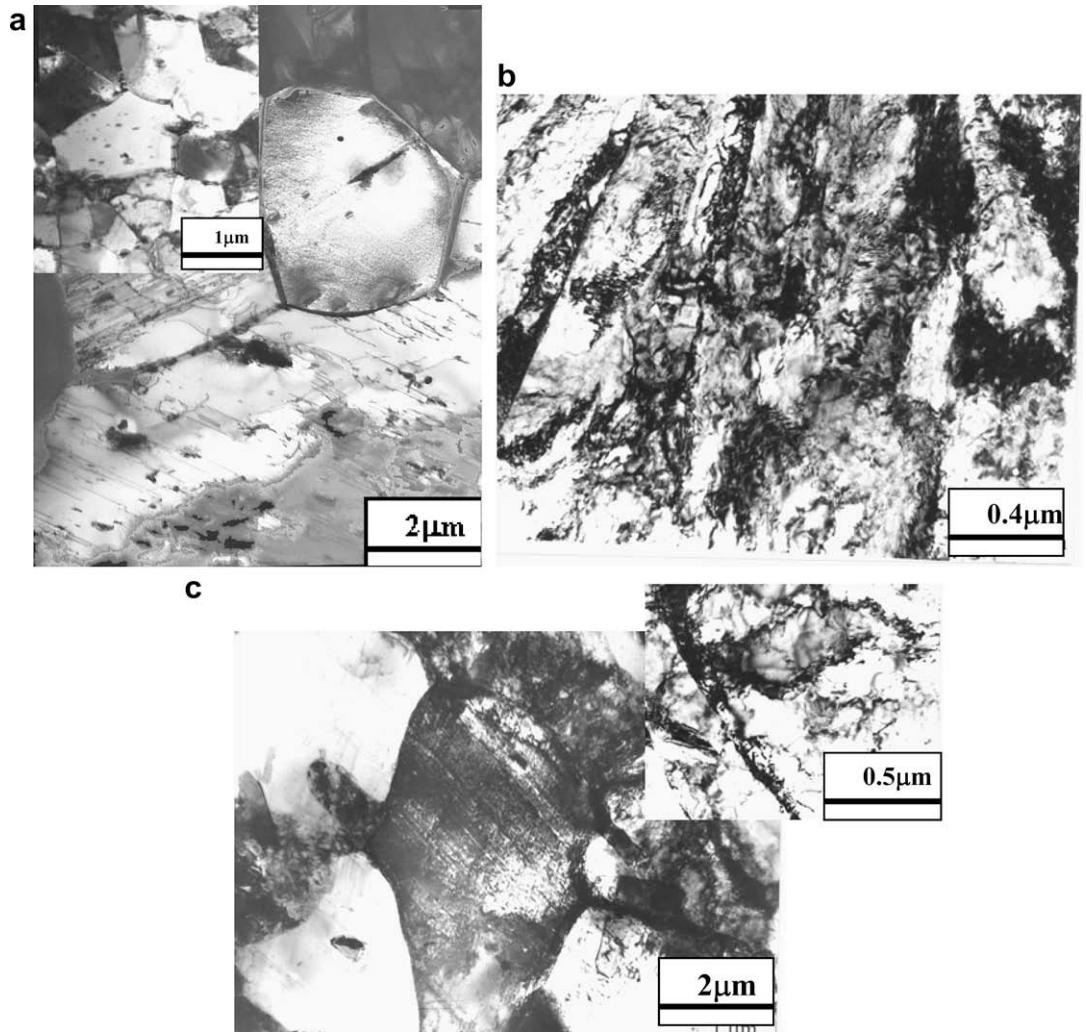

Fig. 7. TEM bright field micrographs (a) 'hot extruded', (b) 'first pilgered' and (c) 'final annealed'. Inset of (a) shows finer grains of hot extruded structure. The inset of (c) is a high magnification picture of deformed region of 'final annealed' structure.

Table 2
Difference in crystallographic and morphological features between smaller and larger grains of hot extruded microstructure

Feature	Larger grains	Smaller grains
Average grain size	20 μm	10 μm
Volume fraction	15%	85%
Morphology	Elongated in the direction of extrusion. (aspect ratio ranged from 2 to 3)	Largely equiaxed (aspect ratio close to 1)
Grain average misorientation (GAM)[a]	0.7°	0.3°
Texture index[b]	400	150

[a] GAM is defined as average misoreitnation between different points in the same grain.
[b] Texture index is a scalar quantity representing the degree of texturing or anisotropy. It is defined as $\int f(g)^2 dg$, where $f(g)$ is ODF (orientation distribution function) intensity and g is an orientation [27].

Also in case of annealing, larger recrystallized grains appear to have defined the evolution of crystallographic texture better – see Fig. 6. In recrystallization of cubic materials, the development in crystallographic texture is often viewed as frequency and/or size advantage of grains of particular orientation(s) [35,36,38,39]. This has been considered as a better means of describing the final recrystallized microstructure – a convention which does not get 'bogged' into the classical controversies [35–37] of orientated nucleation and orientation growth. Interestingly, in hexagonal zirconium, studies on recrystallization texture developments, especially on recrystallization micromechanisms, are 'limited'. It appears, based on the present results of the annealing stages in Zircaloy-4, that the size advantage of the recrystallized grains largely defined textural developments. If such a size advantage is due to competitive growth, or through nucleation [38] and/or microgrowth advantage/selection [40], remains to be established.

Explaining 'hot extrusion' texture/microstructure is difficult as hot extrusion is a complex process involving deformation, recrystallization (static and dynamic) and possible phase transformation. It needs to be noted that the stated extrusion temperature makes the material predominantly single phase. Such an estimate, however, does not take into account possible local temperature variations and also differences in phase concentrations due to solute partitioning. The bimodal grain size distribution observed in the present zirconium has one 'analogy' – hot worked microstructure of transformer steel [41,42]. Typical hot band structure of transformer steel consists of bimodal grain size/shape – finer grains are normally thought to be originating from local phase transformations (ferrite to austenite and back) caused by carbon segregation (otherwise Fe−3.2 wt% Si exists only in single phase). A similar analogy, i.e. local transformation of hcp to bcc and back, can be brought in for the hot extruded microstructure of the present Zircaloy-4. Such an analogy, though speculative at this stage, will explain randomized orientations (see Table 2) of the smaller hot extruded grains. However, inhomogeneous microstructures may also arise through localized variations in hot deformation, with activation of different slip systems, and static/dynamic recrystallization. Though the present study could bring in the importance of hot extrusion in the overall textural/microstructural developments, it is fair to admit that identification of the exact micromechanism(s) of the formation of the hot extruded structure remains inconclusive at this stage.

5. Conclusions

The present study attempts to quantify developments in crystallographic texture and in microstructure/microtexture at different stages of fabrication of Zircaloy-4 fuel tube. Following points summarize the observations.

1. Textural developments during fabrications steps were generalized as developments in $\langle 10\bar{1}0\rangle$ and (0001) fibers. In general, deformation (both hot extrusion, as well as pilgering) strengthened $\langle 1\bar{1}00\rangle$, while annealing enhanced (0001). Only exception to this generalized pattern was the third pilgering step (step with highest '*q*' and lowest reduction), where enhancement of $\langle 10\bar{1}0\rangle$ fiber was insignificant.
2. The processing steps also modified microstructure in the following sequence : Widmanstätten structure (β-quenched) → - bimodal grain size/shape (hot extruded) → relative grain growth (first annealing) → heterogeneous deformation (first pilgered) → fully recrystallized (second annealed) → heterogeneous deformation (second pilgered) → partially recrystallized (third annealed) → heterogeneous deformation (third pilgered) → partially recrystallized (final annealed). Textural developments were associated with grain size – larger grains, in general, had a stronger contribution to textural evolution, observed in case of both deformation as well as annealing.
3. The pilgering operations involved heterogeneous deformation – majority of the grains were fragmented, while some specific grains/orientations were relatively unaffected. Textural developments were observed to be associated with the latter. During annealing, involving complete or partial recrystallization, larger recrystallized grains had a stronger contribution to the developments of crystallographic texture.

Acknowledgements

The authors acknowledge BRNS (Board of Research in Nuclear Sciences, India) for financial support. The use of the National Facility of Texture and OIM, a DST (Department of Science and Technology, India)- supported facility, at IIT Bombay, is also appreciated.

References

[1] K. Linga Murty, Indrajit Charit, Prog. Nucl. Energy 48 (2006) 325.
[2] C. Ganguly, Advances in Zirconium Technology for Nuclear reactor application: ZIRC-2002, Mumbai, India, 2002.
[3] B.A. Cheadle, C.E. Coleman, H. Litcht, Nucl. Technol. 57 (1982) 413.
[4] B.A. Cheadle, Zirconium in Nuclear Industry, ASTM STP 633, Philadelphia, vol. 457, 1977.
[5] K. Videm, L. Lunde, ASTM-STP 681 (1979) 229.
[6] B. Cox, ASTM-STP 681 (1979) 306.
[7] R.A. Holt, E.F. Ibrahim, Acta. Matall. 27 (1979) 1319.
[8] K.V. Mani Krishna, A. Sain, I. Samajdar, G.K. Dey, D. Srivastava, S. Neogy, R. Tewari, S. Banerjee, Acta Mater. 54 (2006) 4665.
[9] V. Perovic, G.C. Weatherly, C.J. Simpson, Acta Metall. 31 (1983) 1381.
[10] C.E. Coleman, D. Hardie, J. Nucl. Mater. 19 (1966) 1.
[11] Young Suk Kim, Yuriy Perlovich, Margarita Isaenkova, S.S. Kim, Yong Moo Cheong, J. Nucl. Mater. 297 (2001) 292.
[12] G. Osterberg, J. Nucl. Mater. 40 (1971) 53.
[13] J.J. Kearns, C.R. Woods, J. Nucl. Mater. 20 (1966) 241.
[14] Sung Soo Kim, Sang Chun Kwon, Young Suk Kim, J. Nucl. Mater. 273 (1999) 52.
[15] E. Technoff, ASTM STP-966, ASTM, Philadelphia, 1980.
[16] Ayesha J. Haq, A. Haq, S. Banerjee, Bull. Mater. Sci. 15 (1992) 289.
[17] Krister Kallstrom, Can. Metall. Quart. 11 (1972) 185.
[18] D. Srivastava, G.K. Dey, S. Banerjee, Metall. Trans. 26A (1995) 2707.
[19] M.J. Luton, J.J. Jonas, Can. Metall. Quart. 11 (1972) 79.
[20] D.J. Abson, J.J. Jonas, J. Nucl. Mater. 42 (1972) 7.
[21] A.M. Garde, H.M. Chung, T.F. Kassner, Acta Metall. 26 (1978) 153.
[22] D. Lee, W.A. Backofen, Trans. AIME 239 (1967) 1034.
[23] B.N. Mehrotra, K. Tangri, Acta Metall. 28 (1980) 1385.
[24] M. Kiran Kumar, C. Vanitha, I. Samajdar, G.K. Dey, R. Tewari, D. Srivastava, S. Banerjee, J. Nucl. Mater. 335 (2004) 48.
[25] E. Tenckhoff, Metall. Trans. 9A (1978) 1401.
[26] E. Tenckhoff, J. ASTM Int. 2 (2005) 1.
[27] S.K. Yerra, B. Verlinden, P. Van Houtte, Mater. Sci. Forum 495 (2005) 913.
[28] J.K. Chakravartty, S. Banerjee, Y.V.R.K. Prasad, M.K. Asundi, J. Nucl. Mater. 187 (1992) 260.

[29] J.K. Chakravartty, Y.V.R.K. Prasad, M.K. Asundi, Metall. Trans. (A) 22 (1991) 829.
[30] Y.V.R.K. Prasad, H.L. Gegel, S.M. Doraivelu, J.C. Malas, J.T. Norgan, K.A. Lark, D.R. Barker, Metall. Trans. (A) 15 (1984) 1883.
[31] H.L. Gegel, J.C. Malas, S.M. Doraivelu, V.A. Shende, Metals Hand Book, vol. 14, American Society for Metals, Metals Park, Ohio, 1987. p. 471.
[32] K.L. Murty, B.L. Adams, ASTM STP 765 (1982).
[33] R.G. Ballinger, G.E. Lucas, R.M. Pelloux, J. Nucl. Mater. 126 (1984) 53.
[34] S.K. Sahoo, V.D. Hiwarkar, I. Samajdar, G.K. Dey, D. Srivastava, R. Tiwari, S. Banerjee, Scripta Mater. 56 (2007) 963.
[35] R.D. Doherty, Scripta Metall. 19 (1985) 927.
[36] R.D. Doherty, D.A. Hughes, F.J. Humphreys, J.J. Jonas, Juul D. Jensen, M.E. Kassner, W.E. King, T.R. McNelley, H.J. McQueen, A.D. Rollett, Mater. Sci. Eng. A 238 (1997) 219.
[37] F.J. Humphreys, M. Hatherly, Recrystallization and Related Annealing Phenomena, Elsevier Science Limited, UK, 1995.
[38] I. Samajdar, R.D. Doherty, Acta Mater. 46 (1998) 3145.
[39] I. Samajdar, B. Verlinden, P. Van Houtte, Acta Mater. 46 (8) (1998) 2751.
[40] B.J. Duggan, K. Lücke, G. Köhlhoff, C.S. Lee, Acta Metall. 41 (1993) 1921.
[41] M. Matsuo, ISIJ Int. 29 (10) (1989) 809.
[42] S. Cicalè, I. Samajdar, B. Verlinden, G. Abbruzzese, P. Van Houtte, ISIJ Int. 42 (7) (2002) 770.